AIAA JOURNAL
Vol. 49, No. 6, June 2011

Transonic Aeroelastic Stability Analysis Using a Kriging-Based Schur Complement Formulation

S. Timme,* S. Marques,† and K. J. Badcock‡
University of Liverpool, Liverpool, England L63 3GH, United Kingdom

DOI: 10.2514/1.J050975

A method is described to allow searches for transonic aeroelastic instability of realistically sized aircraft models in multidimensional parameter spaces when computational fluid dynamics are used to model the aerodynamics. Aeroelastic instability is predicted from a small nonlinear eigenvalue problem. The approximation of the computationally expensive interaction term modeling the fluid response is formulated to allow the automated and blind search for aeroelastic instability. The approximation uses a kriging interpolation of exact numerical samples covering the parameter space. The approach, demonstrated for the Goland wing and the multidisciplinary optimization transport wing, results in stability analyses over whole flight envelopes at an equivalent cost of several steady-state simulations.

Nomenclature

A	=	Jacobian matrix
$\boldsymbol{c}$	=	real-valued constant vector
D, E	=	matrices in modal structural model
$\boldsymbol{f}$	=	vector of aerodynamic forces
I	=	identity matrix
i	=	imaginary unit ($\sqrt{-1}$)
M, C, K	=	mass, damping, and stiffness matrices
m	=	number of parameter dimensions
M_r	=	freestream Mach number
n	=	number of normal modes, number of unknowns
$\boldsymbol{p}$	=	eigenvector
$\boldsymbol{R}$	=	residual vector
S	=	Schur complement matrix ($A_{ss} + S^c$)
S^c	=	interaction term of Schur complement matrix
$\boldsymbol{w}$, $\dot{\boldsymbol{w}}$	=	vectors of unknowns and corresponding temporal derivative
$\boldsymbol{x}$, $\dot{\boldsymbol{x}}$	=	vectors of fluid mesh locations and velocities
Y	=	solution matrix of linear system
$\boldsymbol{y}$	=	solution vector of linear system
α	=	angle of attack
$\boldsymbol{\eta}$, $\dot{\boldsymbol{\eta}}$	=	vectors of generalized coordinates and velocities
ϑ	=	mass ratio
λ	=	eigenvalue
μ	=	bifurcation parameter
σ	=	eigenvalue real part
Φ	=	matrix of mode shape vectors
ω	=	eigenvalue imaginary part, circular frequency

Subscripts

f	=	fluid
s	=	structural
ε	=	small variation
0	=	steady-state or mean value

Presented as Paper 2010-8228 at the AIAA Atmospheric Flight Mechanics Conference, Toronto, 2–5 August 2010; received 5 October 2010; revision received 7 January 2011; accepted for publication 4 February 2011.

*Research Associate, Computational Fluid Dynamics Laboratory, School of Engineering; Sebastian.Timme@liverpool.ac.uk. Member AIAA.

†Research Associate, Computational Fluid Dynamics Laboratory, School of Engineering. Member AIAA.

‡Professor, Computational Fluid Dynamics Laboratory, School of Engineering; K.J.Badcock@liverpool.ac.uk. Senior Member AIAA.

I. Introduction

THE prediction of aeroelastic instability is a critical engineering challenge in aircraft design and certification. Standard approaches in industrial applications are the classical k and p-k methods [1]. These use an inviscid linearized theory formulated in the frequency domain to determine the unsteady aerodynamic response to modal motions. The doublet lattice method has been the single most important tool in production flutter analyses for 40 years [2]. Modern aircraft routinely operate in the transonic regime with its mixed subsonic and supersonic regions, where a linear aerodynamic theory formally fails due to the presence of flow nonlinearities, such as shock waves and shock-induced flow separation. The linear numerical predictions have to be corrected with data from experimental campaigns or higher-fidelity flow simulations [3,4].

Transonic aerodynamics have to be modeled by nonlinear equations for satisfactory results [5]. The use of computational aeroelasticity employing high-fidelity aerodynamics based on computational fluid dynamics (CFD) has matured from a research exercise to a powerful tool in engineering applications due to advances in algorithms and computer power over the last four decades [6]. The stability of an aeroelastic system can be inferred from time-accurate simulations following an initial excitation [7,8]. This approach is very capable due to its generality in dealing with dynamically nonlinear systems, while the significant cost of CFD simulations to solve for the unsteady nonlinear transonic aerodynamics is a major drawback, thus in practice limiting the analysis to a few carefully chosen cases. This is exacerbated by the requirement to search a space of system parameters and flight conditions for critical conditions.

To obviate the cost involved in solving large systems with millions of degrees of freedom and to permit routine calculations over the flight envelope, alternative approaches have been investigated over the last decade. One direction, referred to as reduced-order modeling, extracts key data on the dynamic aeroelastic system to form a low-dimensional problem that tries to keep the accuracy of the full-order formulation. Approaches include proper orthogonal decomposition [9–11] and system identification based on the Volterra theory [12,13]. A second direction keeps the (spatial) order of the full system while manipulating its solution procedure to reduce the cost. One popular approach is the harmonic balance method [14,15], giving a reduction in the computational cost associated with simulating dynamically nonlinear time-periodic unsteady problems, such as limit-cycle oscillation (LCO). Another approach, presented in this work, uses the theory of dynamical systems to predict

aeroelastic instability of the Hopf type, which leads to flutter or LCO. Here, a (linear) stability problem for a (nonlinear) steady-state solution of the aeroelastic system is examined as an alternative to unsteady simulations.

Following an approach first published in [16,17], the solution of an augmented system of equations for the bifurcation point, defining the onset of the aeroelastic instability, was successfully tested on a pitch-and-plunge aerofoil configuration and the flexible AGARD 445.6 wing [18,19]. However, the CFD-based aeroelastic system is typically large, making it difficult to solve the augmented system for the bifurcation point directly. Consequently, several developments have been made since this early work.

First, the shifted inverse power method was adapted to allow the tracing of the aeroelastic modes, starting out in the wind-off structural system and typically defining the instability, with changing values of the bifurcation parameter (i.e., a representation of the dynamic pressure). This provides information about the damping and frequency of the aeroelastic modes [20]. Second, an improved version of the basic method used the Schur complement eigenvalue formulation for enhanced computational performance while avoiding numerical problems associated with the shifted inverse power method [21]. This method was applied to several wing structures and complete aircraft configurations [22,23]. The coupled aeroelastic system is viewed as a modified structural eigenvalue problem with the interaction term, which depends on the response frequency and the parameters defining the steady-state solution, correcting for the aerodynamic influence. The evaluation of the interaction term incurs most of the involved cost, as it generally requires operations on the high-dimensional CFD-based system.

Third, the approximation of this interaction term was formulated (for aerofoil cases) to search parameter spaces for aeroelastic instability and to exploit a hierarchy of nonlinear aerodynamic models, with cheaper models being used to evaluate possible conditions of interest for more expensive models, the evaluation of which is then used to update the approximation [24]. The approximation of the interaction term, using the kriging interpolation based on true numerical samples covering the parameter space of interest, made the Schur complement eigenvalue method essentially a reduced-order model with the unmodified full-order fluid response projected onto the structural system. This paper extends the ideas associated with reconstructing the interaction matrix to three-dimensional test cases under matched point conditions.

The paper continues with the details of the aeroelastic stability analysis. The aerodynamic and structural models used are described, and the Schur complement eigenvalue method including the generation and approximation of the interaction matrix is outlined. A method for coordinated risk-based sampling is shown. The aeroelastic stability analyses for the Goland and multidisciplinary optimization (MDO) wings are presented to illustrate the approach.

II. Governing Equations

A. Flow Model

In the current paper, the Euler equations are used as the aerodynamic model. The governing equations are solved with an established research code [25]. The code uses a block-structured cell-centered, finite volume scheme for spatial discretization. Convective fluxes are evaluated by the approximate Riemann solver of Osher and Chakravarthy [26] with the MUSCL scheme [27], achieving essentially second-order accuracy, and van Albada's limiter, preventing spurious oscillations around steep gradients. Boundary conditions are enforced using two layers of halo cells.

Spatial discretization leads to a system of n_f first-order ordinary differential equations in time written in semidiscrete notation as $\dot{\boldsymbol{w}}_f = \boldsymbol{R}_f(\boldsymbol{w}_f, \boldsymbol{w}_s)$, where $\boldsymbol{w}$ denotes vectors of unknowns and $\boldsymbol{R}_f$ is the fluid residual vector. The subscripts f and s denote fluid and structural contributions, respectively, with the latter contribution influencing the fluid response due to the moving fluid mesh in unsteady simulations. Implicit time marching converges to steady-state solutions, while a second-order dual time stepping is used for unsteady simulations [28]. Resulting linear systems are solved by a preconditioned Krylov subspace iterative method [20].

The eigenvalue stability analysis requires the evaluation of the Jacobian matrix blocks. The fluid Jacobian matrix $A_{ff} = \partial \boldsymbol{R}_f / \partial \boldsymbol{w}_f$ describes the influence of the fluid unknowns on the fluid residual and has, by far, the largest number of nonzero elements for a modal structural model. This matrix block is evaluated analytically (and stored explicitly), which is crucial for the efficiency of the scheme [20]. The matrix block $A_{fs} = \partial \boldsymbol{R}_f / \partial \boldsymbol{w}_s$, describing the dependence of the fluid residual on the moving fluid mesh, is formed using finite differences.

B. Modal Structural Model

Commonly in computational aeroelasticity, an aircraft structure is represented as a linear combination of normal modes, small in number when compared with the large dimension of the CFD system. The deflections $\delta \boldsymbol{x}_s$ of the (linear) structure are defined at a set of points $\boldsymbol{x}_s$ by $\delta \boldsymbol{x}_s(t) = \Phi(\boldsymbol{x}_s)\boldsymbol{\eta}(t)$, where the vector $\boldsymbol{\eta}$ contains the n generalized coordinates (modal amplitudes). The columns of the matrix Φ contain the mode shape vectors evaluated from a finite element model of the structure. The finite element equations are projected onto the mode shapes, and an appropriate scaling is applied to obtain generalized masses of magnitude one according to $\Phi^T M \Phi = I$.

A system of $n_s = 2n$ scalar equations is given for the modal structural model in state-space representation, written as $\dot{\boldsymbol{w}}_s = \boldsymbol{R}_s(\boldsymbol{w}_f, \boldsymbol{w}_s)$, with $\boldsymbol{w}_s = [\boldsymbol{\eta}^T, \dot{\boldsymbol{\eta}}^T]^T$ containing the generalized coordinates and their velocities. The corresponding residual vector is written as $\boldsymbol{R}_s = D\boldsymbol{w}_s + \vartheta E \Phi^T \boldsymbol{f}(\boldsymbol{w}_f, \boldsymbol{w}_s)$, with the matrices $D = [0, I; -\Phi^T K \Phi, -\Phi^T C \Phi]$ and $E = [0, I]^T$, where I is the $n \times n$ identity matrix. The generalized stiffness matrix $\Phi^T K \Phi$ contains the n normal mode frequencies squared on the diagonal. The generalized damping matrix $\Phi^T C \Phi$ contains the n values of modal damping on the diagonal. For the test cases discussed in this paper, structural damping is not considered and is set to zero throughout. The vector $\boldsymbol{f}$ of aerodynamic (pressure) forces at the structural grid points follows from the wall pressure, the area of the surface segment, and the unit normal vector. It is then projected using the modes shapes to obtain the n generalized forces $\Phi^T \boldsymbol{f}$. The mapping between the fluid and structural meshes uses the constant volume tetrahedron transformation [29], although other methods can be used. The parameter ϑ for the mass ratio is obtained from the nondimensionalisation of the governing equations and depends on the reference density.

As for the flow models, the evaluation of the Jacobian matrix blocks is required for the eigenvalue stability analysis. The structural Jacobian matrix $A_{ss} = \partial \boldsymbol{R}_s / \partial \boldsymbol{w}_s$ is split into two contributions, one from the normal mode frequencies and structural damping and one due to the aerodynamic force vector, and it is given by $A_{ss} = D + \vartheta E \Phi^T \partial \boldsymbol{f} / \partial \boldsymbol{w}_s$. From experience, the second term is usually negligible but can easily be included in the calculation. The Jacobian matrix block $A_{sf} = \partial \boldsymbol{R}_s / \partial \boldsymbol{w}_f$ describes how the structure responds to changes in the flow field and is formed as $A_{sf} = \vartheta E \Phi^T \partial \boldsymbol{f} / \partial \boldsymbol{w}_f$. Currently, the evaluation of the derivatives $\partial \boldsymbol{f} / \partial \boldsymbol{w}_s$ and $\partial \boldsymbol{f} / \partial \boldsymbol{w}_f$ is done using finite differences.

III. Eigenvalue Stability Formulation

A. Schur Complement Eigenvalue Method

The aeroelastic system is written in standard state-space form as $\dot{\boldsymbol{w}} = \boldsymbol{R}(\boldsymbol{w}, \mu)$, with the vectors of unknowns $\boldsymbol{w}$ and corresponding residuals $\boldsymbol{R}$ containing fluid and structural contributions and the bifurcation parameter μ in this paper either expressing freestream velocity or altitude. The expression $\boldsymbol{R}(\boldsymbol{w}_0, \mu) = 0$ is satisfied by an equilibrium solution $\boldsymbol{w}_0$ of the nonlinear system. Linear stability is determined by eigenvalues $\lambda = \sigma \pm i\omega$ of the system Jacobian matrix $A(\boldsymbol{w}_0, \mu)$ evaluated at the steady-state and chosen values of μ. More important, the Jacobian matrix is exact with respect to the applied spatial discretization scheme. A stable system has all of its eigenvalues with a negative real part. A pair of complex conjugate

eigenvalues with a zero real part defines the onset of an instability of the Hopf type leading to flutter.

Linear aeroelastic instability can be predicted by solving the standard eigenvalue problem $(A - \lambda I)\boldsymbol{p} = 0$, where the Jacobian matrix is conveniently partitioned in blocks expressing the different dependencies:

$$A = \frac{\partial \boldsymbol{R}}{\partial \boldsymbol{w}} = \begin{pmatrix} A_{ff} & A_{fs} \\ A_{sf} & A_{ss} \end{pmatrix} \tag{1}$$

Partitioning the eigenvector $\boldsymbol{p}$ into vectors of fluid and structural contributions, the Schur complement eigenvalue method [21] is derived. The equation $(S(\lambda) - \lambda I)\boldsymbol{p}_s = 0$ defines a small nonlinear eigenvalue problem for the stability analysis, with the Schur complement matrix $S(\lambda)$ explicitly written as

$$S(\lambda) = A_{ss} - A_{sf}(A_{ff} - \lambda I)^{-1}(A_{f\eta} + \lambda A_{f\dot{\eta}}) \tag{2}$$

where λ is an eigenvalue of the structural part in the uncoupled system. Keeping only the first term on the right-hand side (i.e., the matrix A_{ss}) gives the structural eigenvalue problem, while the second part describes the interaction (coupling) term, $S^c = -A_{sf}(A_{ff} - \lambda I)^{-1}(A_{f\eta} + \lambda A_{f\dot{\eta}})$. As the interaction goes to zero, the structural eigenvalue problem is restored.

The matrix $A_{fs} = [A_{f\eta}, A_{f\dot{\eta}}]$ has been rearranged to illustrate the dependence of the fluid residual $\boldsymbol{R}_f(\boldsymbol{w}_f, \boldsymbol{x}, \dot{\boldsymbol{x}})$ on the structural unknowns with generalized coordinates $\boldsymbol{\eta}$ (according to the structural degrees of freedom) and their velocities $\dot{\boldsymbol{\eta}}$ influencing the grid displacements $\boldsymbol{x}(\boldsymbol{\eta})$ and grid velocities $\dot{\boldsymbol{x}}(\dot{\boldsymbol{\eta}})$ of the fluid mesh. This relation can be seen by observing that, for the state-space representation, the structural eigenvector is written as $\boldsymbol{p}_s = [\boldsymbol{p}_\eta^T, \lambda \boldsymbol{p}_\eta^T]^T$, using the expression $\boldsymbol{\eta} = \boldsymbol{p}_\eta e^{\lambda t}$, consistent with a linear stability analysis [30].

To solve this small complex-valued eigenvalue problem, the system is augmented to scale the structural eigenvector $\boldsymbol{p}_s$ against an arbitrary real-valued constant vector $\boldsymbol{c}_s$. Then, the augmented nonlinear system of the Schur residual is solved for the unknowns $[\boldsymbol{p}_s^T, \lambda]^T$. While the full eigenvalue problem for the matrix A contains $n_f + n_s + 1$ unknowns, the Schur complement eigenvalue formulation only has dimension $n_s + 1$, where the number of the structural unknowns is generally small.

An efficient way of finding the roots of nonlinear systems is the Newton method, which requires the evaluation of the residual and its Jacobian matrix (or an approximation). The evaluation of the interaction term S^c is the main cost, as it involves operations on the high-dimensional fluid system, whereas the cost to form the structural Jacobian matrix A_{ss} is negligible in comparison. The interaction term in the Schur residual is evaluated by first forming the product $(A_{f\eta} + \lambda A_{f\dot{\eta}})\boldsymbol{p}_\eta$ for the current approximation to the eigenvector and then solving one linear system, $(A_{ff} - \lambda I)\boldsymbol{y} = (A_{f\eta} + \lambda A_{f\dot{\eta}})\boldsymbol{p}_\eta$, the solution of which is multiplied with the matrix A_{sf}. Applying finite differences gives the Schur Jacobian matrix. Resulting linear systems are solved throughout in this work using the generalized conjugate residual algorithm [31] with a block incomplete lower/upper factorization (allowing one level of fill-in) as preconditioner. Details can be found in [21,20].

As there are n relevant solutions of the nonlinear eigenvalue problem, the cost of forming the interaction term at each Newton iteration for each value of the independent parameter and for a range of system parameters becomes too high without approximations. Thus, a series approximation [32] of the Schur complement matrix can be written for $\lambda = \lambda_0 + \lambda_\varepsilon$ as

$$\begin{aligned} S(\lambda) \approx A_{ss} - A_{sf}((A_{ff} - \lambda_0 I)^{-1} \\ + \lambda_\varepsilon (A_{ff} - \lambda_0 I)^{-2})(A_{f\eta} + \lambda_0 A_{f\dot{\eta}} + \lambda_\varepsilon A_{f\dot{\eta}}) \end{aligned} \tag{3}$$

where λ_ε denotes a small variation to the reference value λ_0, which is, for instance, a purely imaginary number of magnitude given by a structural frequency or a previously converged solution at a different value of the bifurcation parameter. Precomputing the factors in the series (requiring $4n$ linear solves per shift λ_0 for the first-order expansion) allows the application of the expansion in the vicinity of λ_0. Two approaches have been discussed [21,23]. The quasi-Newton method evaluates the (exact) residual by the nonlinear approach given in the previous paragraph, while the series expansion is used for the Schur Jacobian matrix. The series method also applies the series expansion to the residual, which is possible for small λ_ε and for the bifurcation parameter μ not affecting the precomputed values (i.e., for symmetric problems).

B. Approximation Model

Assuming a simple harmonic motion with constant amplitude for the interaction term, the Schur complement matrix S in Eq. (2) is written as

$$S \approx (C_1 + \vartheta C_2) - \vartheta C_3 (A_{ff} - i\omega I)^{-1}(A_{f\eta} + i\omega A_{f\dot{\eta}}) \tag{4}$$

where the matrices C_1, C_2, and C_3 follow directly from the definition of S in terms of A_{ss} and A_{sf}, given in the previous section. This form allows the evaluation of the matrices C_2 and C_3 independently from the mass ratio ϑ (depending on the reference density), which is convenient for a matched point simulation. The other part of the interaction term, $-C_3(A_{ff} - i\omega I)^{-1}(A_{f\eta} + i\omega A_{f\dot{\eta}})$, is sampled at different locations in the parameter space. In the absence of static aeroelastic deformation, the latter expression is independent of the dynamic pressure reducing the number of relevant parameter dimensions. The matrix $C_1 = D$ also needs to be matched to the current reference values, as the normal mode frequencies are made dimensionless using the reference freestream velocity. The matrix C_2, containing the sensitivities of the force vector with respect to the deformation, is commonly neglected, as it was found to be several (typically three to five) orders of magnitude smaller than the other terms.

Different types of simulations are discussed. First, an altitude can be chosen to set the reference value of the density, and then the freestream velocity (only influencing the matrix C_1 through nondimensionalization) is varied to detect the onset of the instability. The freestream velocity becomes the bifurcation parameter. Second, for a matched point simulation, the altitude (as bifurcation parameter) can be varied independently while adjusting the values of the density and speed of sound according to standard atmosphere conditions. Then, the velocity follows from the freestream Mach number.

The big computational challenge in solving the small nonlinear eigenvalue problem is the evaluation of the Schur interaction matrix S^c to form the Schur residual and Jacobian matrix, as this involves operations on the high-dimensional fluid system. This matrix depends on the eigenvalue, particularly the imaginary part, and the steady-state solution. The steady state makes it dependent on a large number of parameters in both the flow model (e.g., Mach number, angle of attack, and dynamic pressure) and the structural model due to structural parameters generally affecting the mode shapes. This means that the direct evaluation of the matrix S^c (using either of the three described approaches) will become too expensive if a large space of system parameters has to be searched for aeroelastic instability.

For computationally expensive simulations, such as the generation of the Schur interaction matrix, it is useful to generate a cheap approximation based on relatively few runs of the expensive model to provide information about its response at untried parameter combinations. Several approaches to construct response surfaces can be found in the literature. In this study, as introduced in [24], the Schur interaction matrix is reconstructed based on samples (i.e., exact evaluations of this term covering the parameter space of interest) using kriging interpolation. Once the interaction matrix can be represented by the kriging model, the eigenvalue problem can be solved as often as necessary at very low computational cost.

C. Sample Generation

The interaction matrix can be formed in both the frequency and time domains. Solving the n linear systems of the form $(A_{ff} - i\omega I)Y = (A_{f\eta} + i\omega A_{f\dot{\eta}})$ directly and multiplying the solution matrix

Y by the matrix A_{sf} to form the Schur interaction matrix is referred to as the linear frequency domain approach. This is the preferred choice due to the significant computational cost involved in time domain simulations.

Alternatively in the time domain, the interaction matrix (i.e., the generalized aerodynamic influence coefficient matrix) is evaluated from the generalized forces $\Phi^T \boldsymbol{f}$ following an excitation in the structural unknowns. It is straightforward to excite one structural degree of freedom at a time in a forced sinusoidal motion at some fundamental frequency. Then, a column of the interaction matrix is found from the n generalized forces, which are Fourier decomposed and divided by the corresponding Fourier coefficient of the forced structural motion. More elegant and efficient approaches to evaluate the aerodynamic influence from unsteady CFD simulations over a range of frequencies can be used, however, such as an exponentially shaped pulse excitation [33] or unit step/impulse excitation [13,34].

D. Kriging Interpolation

In the kriging interpolation technique, which was described in detail in [35], a multidimensional deterministic response of a simulation is treated as a realization of a stochastic process. This process is composed of a low-order regression model and a random normally distributed signal with zero mean and a covariance, depending on the variance of the input samples and the correlation between two parameter locations. Thus, the second term (the error term) is not independent at different locations but is related to the distance between points in the parameter space. The parameters of the computationally cheap kriging model are determined for a known set of numerical samples of the full-order formulation by an optimization process as given, for instance, in [35,36]. More important, the kriging predictor gives the exact system response at a sampled location. Details of the specific kriging toolbox [37] used in this paper are given in the Appendix.

One representative kriging interpolated element of the Schur interaction matrix S^c for the Goland wing/store configuration with the mass ratio set to unity is shown in Fig. 1. The element describes the response in the first degree of freedom due to changes in the second generalized coordinate. The black dots in the figure indicate sample locations, while the meshed surfaces represent the kriging predictions used for the stability analysis. The two-dimensional parameter space is defined by the dimensionless response frequency and freestream Mach number.

For flutter analyses using linear aerodynamics (such as the doublet lattice method), the aerodynamic influence coefficient matrix is usually evaluated at a limited number of points in the parameter space defined by the reduced frequency and freestream Mach number. This is necessary, as this evaluation significantly contributes to the computational cost. An interpolation is then applied to find the values between these discrete points [38]. Thus, the approach taken in this study is similar but with two important differences. First, nonlinear CFD aerodynamic modeling is applied. Second, the parameter space in the current approach can easily be extended to include more parameter dependencies. Recall that the steady-state solution and, consequently, the interaction matrix can depend on a large number of system parameters.

E. Sampling

The main computational task for the Schur complement eigenvalue method is to evaluate the interaction matrix to describe the fluid response accurately. The goal of this paper is to enable aeroelastic instability searches over the flight envelope, and this is achieved by introducing searches for the approximation of the interaction matrix. Coordinated risk-based sampling was introduced in the previous aerofoil study [24] for two-dimensional parameter spaces including the response frequency and freestream Mach number. Additional input parameter dimensions are now added to demonstrate the generality of the approach. The sampling proceeds in the same fashion as for the aerofoil cases.

First, an initial search space is defined by the corner points, with the frequency range chosen according to the structural frequencies

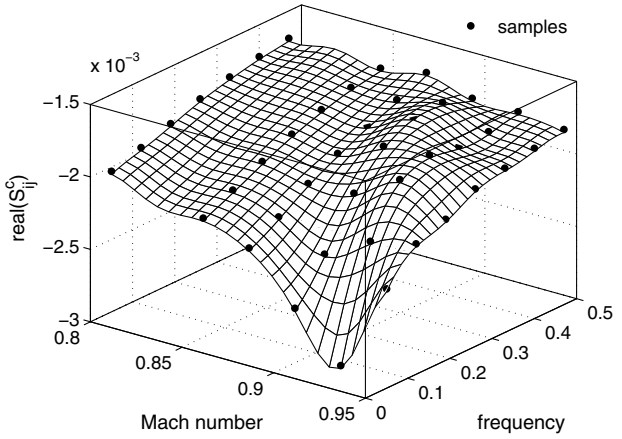

a) Real part

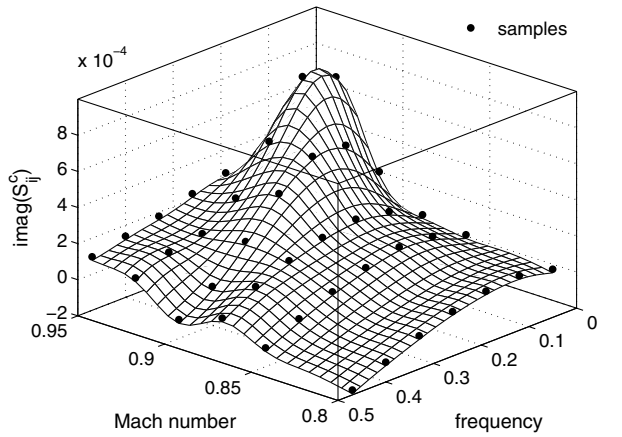

b) Imaginary part

Fig. 1 Extracted and interpolated element $S^c_{5,2}$ of Schur interaction matrix for Goland wing/store configuration using Euler flow model; mass ratio set to unity.

and any additional parameter dependencies chosen according to the region of interest. This gives 2^m initial samples for the m parameter dimensions. Then, the aeroelastic modes from the (wind-off) structural system are traced with varying values of the bifurcation parameter using the kriging model to give the changes in the interaction matrix, and the instability points are detected in the parameter space. This is possible because of the low computational cost of solving the eigenvalue problem with the interaction matrix approximated. More important, the approximation model is always constructed using the most recent set of samples. The detected instability point corresponding to the highest kriging error in the prediction of the interaction matrix gives a new sample location.[§] The prediction error is readily estimated from the kriging model. Such a risk-based sampling guarantees that samples are always placed at locations where they support the prediction most in terms of risk (i.e., at previously evaluated instability points) and improvement (i.e., at the location of the maximum error in the kriging model). Changes in the instability prediction between consecutive iterations give a convergence criterion.

To generalize, risk-based sampling can be outlined step by step as follows:

1) Define initial sampling pattern of parameter space.

2) Iterate until convergence is found.

a) Use full-order CFD tool to calculate the interaction matrix at the chosen parameter location(s).

[§]Alternative sampling criteria, such as a positive gradient in the eigenvalue's real part with respect to the bifurcation parameter, are possible choices. At this point, expert knowledge would need to be inserted to specify possible adaptations of the sampling criterion.

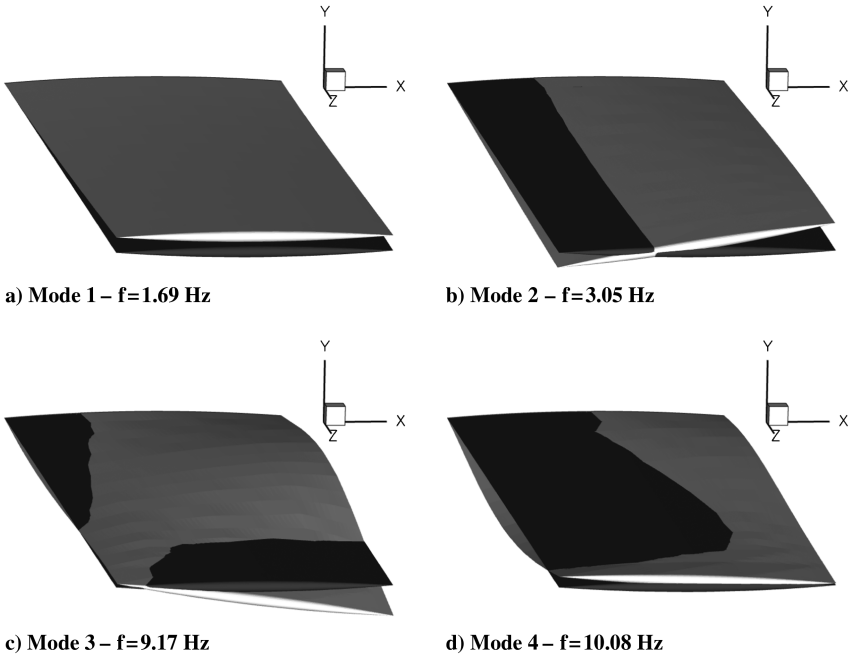

Fig. 2 Mode shapes of baseline Goland wing/store configuration.

b) Form the kriging model based on all available samples to approximate interaction matrix.

c) Run complete stability analysis using the kriging model to obtain critical parameter values.

d) If the iterative solution satisfies user-predefined convergence criteria, stop iterating.

e) Otherwise, choose a new sample location according to user-predefined sampling criteria.

The iteration stage can be made fully automated. Of course, the step involving the application of the CFD tool is the most expensive. Steps involving initial user input allow expert knowledge to be inserted.

IV. Results

In this section, two test cases are discussed: the symmetric Goland wing/store configuration and the nonsymmetric MDO wing configuration accounting for static aeroelastic deformation. For these cases, it is demonstrated that the kriging approximation approach gives stability predictions on a par with the exact full-order eigenvalue solver at lower computational cost when applied over the flight envelope. Furthermore, it is shown how coordinated risk-based sampling allows the aeroelastic instability search in larger parameter spaces while reducing the cost of constructing the approximation model.

A. Goland Wing/Store: Symmetric Case Without Static Aeroelastic Deformation

The Goland wing is a model wing having a chord of 1.8266 m and a span of 6.096 m. It is rectangular and cantilevered with a constant cross section defined by a 4% thick parabolic-arc aerofoil. The finite element model, used to calculate the mode shapes, follows the description given in [39]. The baseline wing/store configuration is discussed retaining the four modes with the lowest frequencies for the aeroelastic simulations. The frequencies as well as the mode shapes mapped to the CFD surface mesh are shown in Fig. 2. A computational mesh with 200,000 control volumes is used for the current Euler simulations. The store aerodynamics are not modeled in this study.

The instability boundary, as critical values of freestream velocity at fixed sea level conditions, is presented in Fig. 3. The instability onset with increasing freestream velocity is compared with the numerical predictions from [39]. The results using the kriging approach are included with the corresponding response surfaces, shown in Fig. 1. The kriging approach gives excellent agreement with the predictions based on the exact eigenvalue solver, where the full-order results using both the quasi-Newton method and the series method were found to be indistinguishable. Good agreement is also seen with the transonic small disturbance (TSD) prediction from [39], while a detailed comparative study (concerning factors like grid resolution and definition of mode shapes) would be required to explain the remaining differences. In the figure, it can be seen that the dominant aeroelastic response changes from the (until then) first bending mode to the first torsion mode at a transonic freestream Mach number of about 0.9. The torsion mode instability is characterized by the bucket of shock-induced LCO. Note that the peaks before and after the bucket of LCO are characterized by the third mode [39].

The results of time-accurate unsteady simulations, included in Fig. 3 at two freestream Mach numbers, are consistent with the eigenvalue predictions, with the plus (tilde) sign indicating a stable (unstable) response due to an initial disturbance in the steady state. In

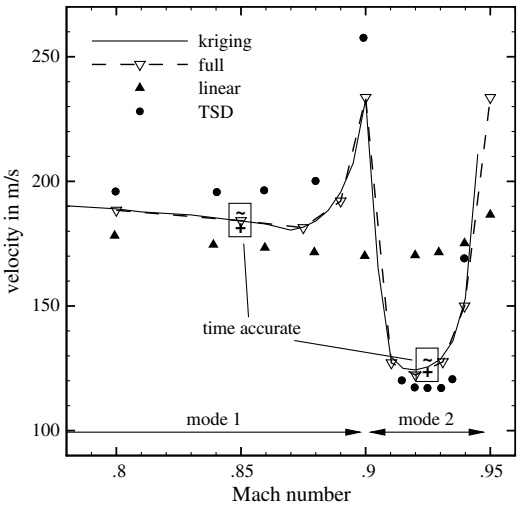

Fig. 3 Instability boundary of Goland wing/store configuration for Euler flow model showing critical values of velocity at sea level conditions: linear denotes linear aerodynamic theory in MSC.Nastran (both linear and TSD are from [39]).

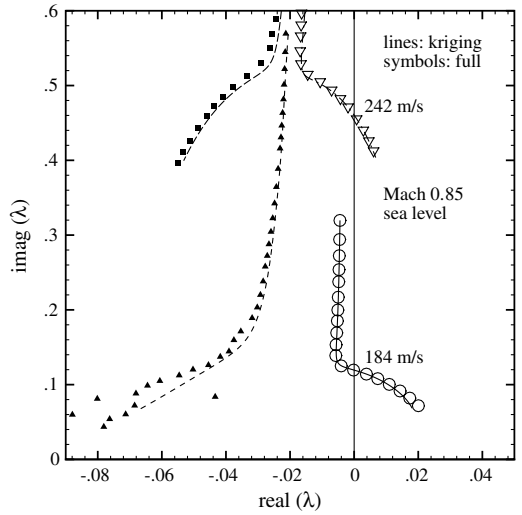

Fig. 4 Mode tracing with respect to velocity at sea level conditions and Mach 0.85 for Goland wing/store configuration using Euler flow model; eigenvalues given in dimensionless form.

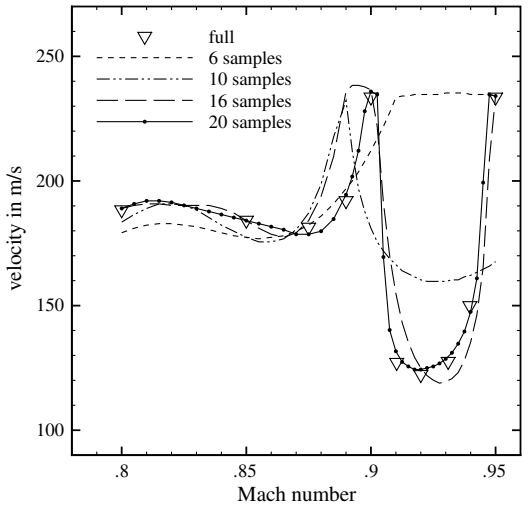

Fig. 5 Risk-based sampling for Goland wing/store configuration showing critical values of velocity at sea level conditions.

contrast with the lower Mach number at 0.85, the response signals of the generalized coordinates (not shown herein) describe a limit-cycle instability strongly dominated by the second mode at Mach 0.925.

Figure 4 shows the root loci of the four aeroelastic modes with respect to velocity changes at a freestream Mach number of 0.85, comparing results from the kriging approach and the exact eigenvalue solver. For the latter predictions, the series method was applied with the series factors reevaluated once the variation λ_ε exceeded one-tenth of the reference λ_0. The results at Mach 0.85 show a classical binary instability mechanism, with an instability occurring alongside the interaction of two aeroelastic modes involving the first bending and first torsion modes. In addition, the configuration gives a second instability at higher velocities following the interaction of the third and fourth modes (which is not included in Fig. 3).

The simplification of using an approximate Schur interaction matrix based on samples for a simple harmonic motion is appropriate, as seen from these results. The modes can be traced accurately, even away from the imaginary axis (where the approximation is exact within the limits of the interpolation algorithm), suggesting that the variation in the purely structural eigenvalue problem, $(A_{ss} - \lambda I)\boldsymbol{p}_s$, with respect to the eigenvalue's real part is more dominant compared with the variation in the interaction term $S^c(\omega)$. The erratic trace of the second mode at Mach 0.85, obtained with the exact eigenvalue solver, reveals a typical problem. As the exact interaction term $S^c(\lambda)$ is evaluated for eigenvalues with a nonzero real part, the eigenvalues from the wind-off structural system can interfere with the eigenvalue spectrum of the fluid system (a characteristic Euler eigenvalue spectrum is shown in [18]) causing an ill-conditioning of Eq. (2). However, for the sample generation applied in this paper, assuming simple harmonic motion (i.e., eigenvalues with zero real part), this does not become an issue for the kriging approach.

For the reconstruction of the response surfaces in Fig. 1, 42 samples are used, corresponding to the cost of $42 \times n$ linear solves against the fluid system once the steady-state solution is available. A linear solve is taken as an equivalent cost unit, because the solutions of the large sparse linear systems incur most of the involved cost, while in this case, the evaluation of three samples corresponds in cost to solving one steady state. To give numbers, the n linear solves per sample (including the evaluation of the Jacobian matrix blocks and preconditioning) are done in about 8 min. of CPU time on a desktop machine while converging the linear residual seven orders of magnitude. These samples allow the stability analysis, covering a range of freestream Mach numbers. Using the series method with a first-order expansion, the evaluation of the series factors (for all four normal modes) takes $n \times 4n$ linear solves per steady state (amounting to about 2 h of CPU time for the 64 linear solves), while tracing the modes can then be done essentially without additional cost. Thus, with the third Mach number, the cost invested in constructing the kriging model pays off. Also, the reconstruction approach becomes more powerful with an increasing number of normal modes, as every individual sample supports the analysis/tracing of all modes, while the series factors are only valid close to the shift λ_0 (e.g., a structural frequency) they have been evaluated for.

Using risk-based sampling, which is presented in Figs. 5 and 6 for the baseline Goland wing/store configuration, the computational cost of the approximation model can be further reduced. Figure 5 shows the convergence of the instability boundary. The instability boundary is accurately predicted with 20 samples. The number of samples required means a further cost reduction by a factor of two in this example, while more significant savings are obtained for the following test case. The distribution of these samples, together with a representative approximated response surface and the projected trace of the instability, is shown in Fig. 6. The clustering of the samples around the converged instability boundary can be seen.

B. Multidisciplinary Optimization Wing: Nonsymmetric Case with Static Aeroelastic Deformation

The MDO wing is a flexible, commercial transport wing designed to operate in the transonic range. It has a span of 36 m and a thick supercritical section. The nonsymmetric section makes the steady-state solution, and hence the interaction term, dependent on the altitude, chosen as the bifurcation parameter. The presented

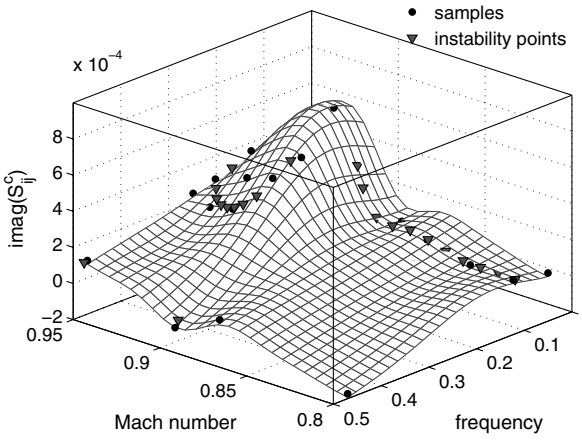

Fig. 6 Risk-based sampling for Goland wing/store configuration showing element $\mathrm{imag}(S^c_{5,2})$ of Schur interaction matrix and using Euler flow model; mass ratio set to unity.

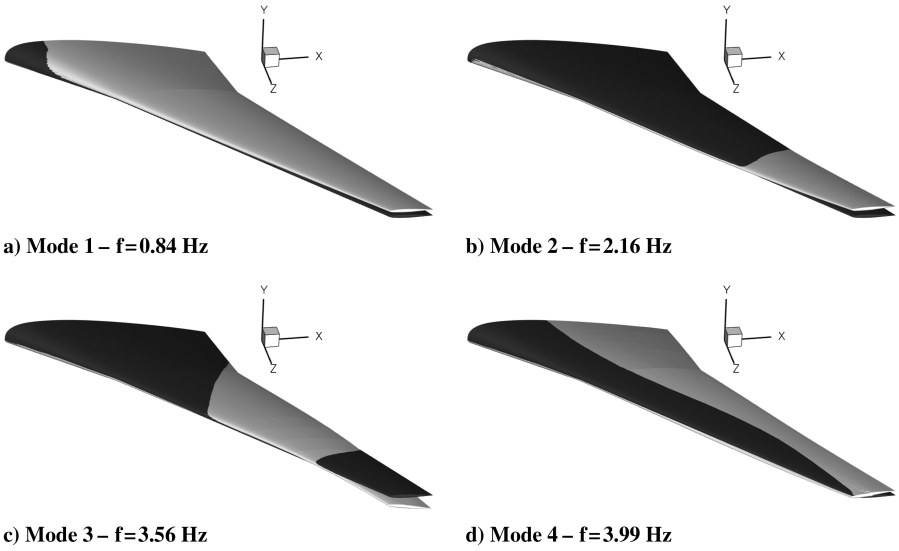

a) Mode 1 – f=0.84 Hz **b) Mode 2 – f=2.16 Hz**

c) Mode 3 – f=3.56 Hz **d) Mode 4 – f=3.99 Hz**

Fig. 7 Mode shapes of MDO wing configuration: modes 1 to 4.

approximation approach becomes very attractive concerning the cost. A computational mesh with 65,000 control volumes is used for the current Euler simulations. The finite element model is given by a wing box along the central portion of the wing [21]. For the aeroelastic stability analysis, eight normal modes are considered, with the mode shapes for the four lowest structural frequencies given in Fig. 7. This case has been chosen to demonstrate the applicability of kriging interpolation for the sampling and reconstruction approach to a higher number of normal modes and independent parameter dimensions.

The challenge for the kriging model as discussed up to this point is not the inclusion of static deformation at a fixed freestream Mach number, giving a two-dimensional parameter space, but the search for aeroelastic instability over the flight envelope (i.e., a range of freestream Mach numbers). This three-dimensional parameter space is analyzed using 256 samples distributed at four (dimensionless circular) frequencies between 0.4 and 2.5, eight altitudes between 0 and 15 km, and eight freestream Mach numbers between 0.7 and 0.88. A slice through this parameter space at a freestream Mach number of 0.85 and a 0 deg angle of attack is given in Fig. 8, showing one element of the interaction matrix as a function of the dimensionless frequency and altitude. The interaction matrix is given with the actual value of the mass ratio depending on the altitude.

The corresponding tracing[¶] of all aeroelastic modes originating in the wind-off structural system is presented in Fig. 9. The figure gives an accurate tracing compared with the full-order results using the series method. Here, the series factors (just as the steady states) were reevaluated at each new altitude for reasons of accuracy, with an applied decrement of 500 m making it quasi Newton. The first mode goes unstable at an altitude of about 4.5 km, closely followed by the second mode crossing the imaginary axis at about 3.8 km. The differences in the frequency at lower altitudes for the fourth mode are due to the strongly damped character of this mode. The assumption of a simple harmonic aerodynamic response [i.e., $S^c(\omega)$ instead of $S^c(\lambda)$] does not hold in this case. However, this behavior is irrelevant for the stability prediction.

The structural model applied in the current formulation is linear. In [40], however, it was argued that, for the class of flexible high-aspect-ratio swept wings (such as the MDO wing), the nonlinear static aeroelastic deformation plays a fundamental role in the instability mechanism, causing a low-amplitude limit-cycle oscillation, which may persist at high altitudes. A nonlinear structural model was required in [40] to capture the described phenomenon, whereas a linear structure resulted in a critical dynamic pressure overpredicted by a factor of three. In terms of applicability of the approach discussed in this paper, it must be remarked that the kriging model is constructed to approximate the results of the exact eigenvalue solver, no matter if a linear or nonlinear structural model is used, and its cost must be judged relative to the exact eigenvalue solver.

The results of the stability analysis in the three-dimensional parameter space showing critical values of altitude are presented in Fig. 10. The agreement between the kriging and full-order series results is close. For freestream Mach numbers below 0.75, the configuration only encounters aeroelastic instability below sea level, while at common cruise conditions, the critical region starts at about 5 km. Within the considered range of freestream Mach numbers, the first mode instability is critical throughout.

The stability limit for the rigid MDO wing (i.e., without static aeroelastic deformation) is included in Fig. 10. These results demonstrate the importance of simulating static deformation in transonic aeroelastic stability analyses. The typical transonic dip, related to the first bending mode instability, is formed and shifted to lower Mach numbers compared with the results including static deformation. This is attributed to the formation of shock waves. The influence of the static deformation on the steady-state solution with varying altitude is presented in Fig. 11 and compared with the results of a rigid wing simulation. The flow is simulated at a fixed transonic freestream Mach number of 0.85 and a 0 deg angle of attack. A decreasing altitude, corresponding to an increase in the dynamic

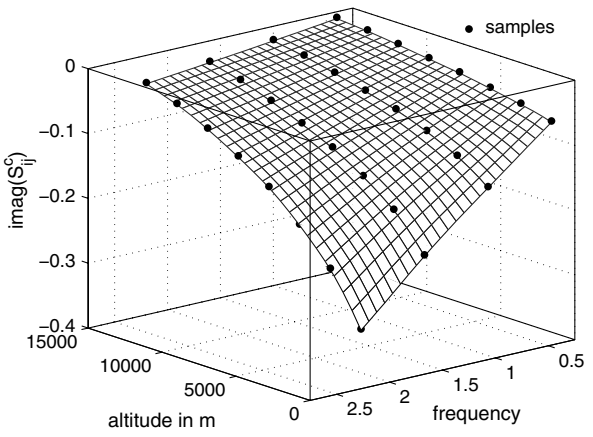

Fig. 8 Extracted and interpolated element $\mathrm{imag}(S^c_{10,1})$ of Schur interaction matrix for MDO wing configuration at Mach 0.85 and 0 deg angle of attack.

[¶]Note that the eigenvalues are not traced starting from an altitude corresponding to zero dynamic pressure but from an altitude of 15 km. Hence, the roots do not start from the imaginary axis.

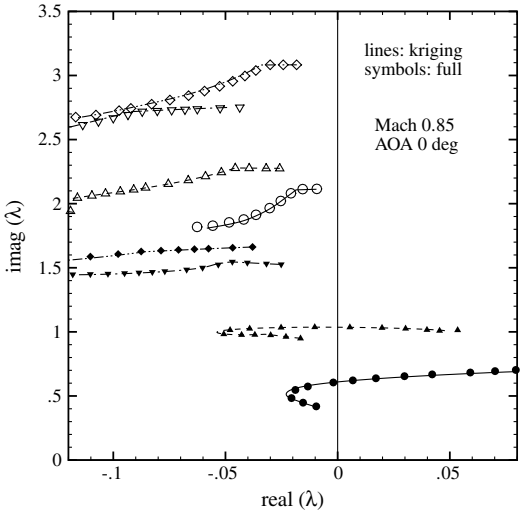

a) Root loci

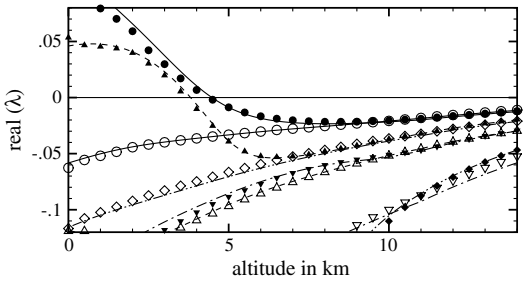

b) Mode damping

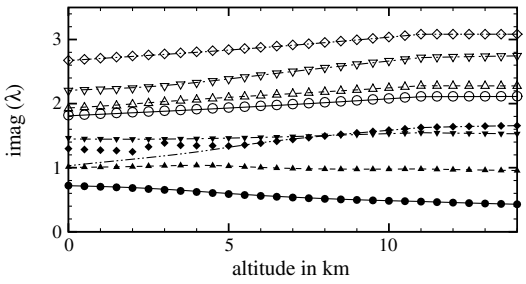

c) Mode frequency

Fig. 9 Mode tracing with respect to altitude for MDO wing configuration at Mach 0.85 and 0 deg angle of attack (AOA); eigenvalues given in dimensionless form.

pressure, causes the wing to bend up and to twist the nose down slightly at the wing tip, resulting in a weakened shock wave on the upper surface of the wing. Thus, the shock strengths are reduced by the static deformation compared with the rigid wing case.

The issue of cost is now considered for the case with static aeroelastic deflection. In the three-dimensional parameter space, 256 samples are used, which is equivalent to the cost of $256 \times n$ linear solves plus the evaluation of the steady state at each altitude/Mach number combination. Evaluating one steady state corresponds in cost to solving approximately $2n$ linear systems (i.e., two samples) in this case. To clarify matters, reducing the nonlinear residual for the steady-state solution five orders of magnitude requires less than 5 min. of CPU time on a modern desktop machine, while the n linear solves per sample are then obtained in about 2 min., converging the linear residual seven orders of magnitude. The achieved resolution of the reconstructed response surfaces is sufficient for accurate predictions compared with the full-order results. Using the exact eigenvalue solver with the series method, the series factors (just as the steady states) have to be recalculated several times as the altitude is decreased due to the altered static deformation. Assume that four

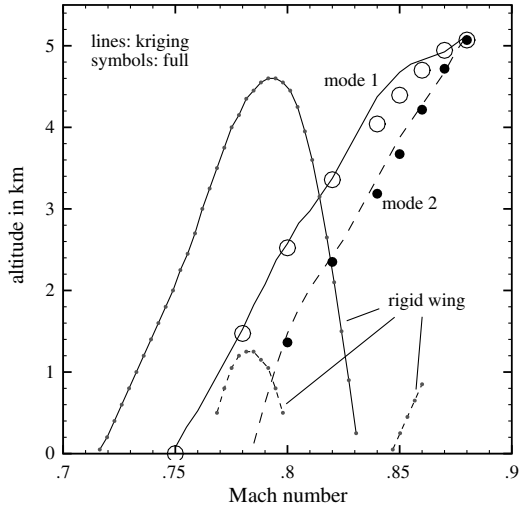

Fig. 10 Stability results for MDO wing configuration using three-dimensional grid sampling showing critical values of altitude.

Mach numbers are to be investigated. If, for an altitude search range of 15 km, the series factors are reevaluated only four times, which clearly introduces inaccuracy in the predictions, an equivalent cost of $4 \times 4 \times n \times 4n$ linear solves for the eight normal modes is created, amounting to about 17 h of CPU time for the 4096 linear solves. The construction of the three-dimensional kriging model generates about half the cost while giving accurate results.

Risk-based sampling can be used to further reduce the overall computational cost, and these results are presented in Figs. 12–14. The search for aeroelastic instability in the frequency/altitude parameter space at a fixed freestream Mach number of 0.85 is shown in Fig. 12. The sampling converges rapidly, as can be seen in the figure, showing a representative element of the interaction matrix together with the sample distribution and the (converged) instability points. After the third iteration, starting from the four initial samples defining the search space, a new sample location matches the predicted instability points of the first and second modes very closely. Continuing to iterate is neither necessary nor useful, as the correlation matrix of the kriging model becomes increasingly ill-conditioned for samples near previously sampled points [35]. Thus, the seven sufficient risk-based samples mean a cost reduction by a factor of about five, compared with the grid sampling shown in Fig. 8.

In Fig. 13, the mode tracing using these seven risk-based samples for the reconstruction of the response surfaces gives excellent agreement with the full-order series method throughout both the

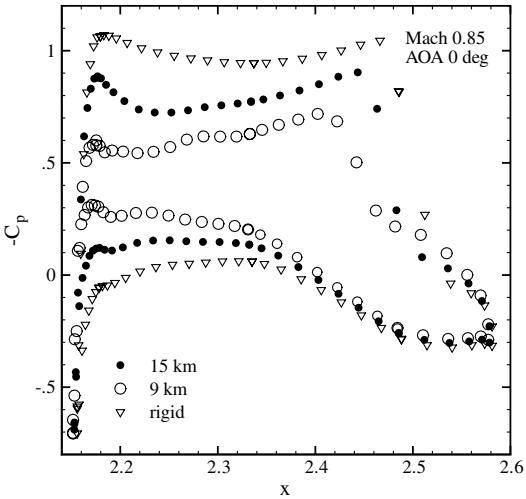

Fig. 11 Effect of static aeroelastic deformation on pressure distribution at wing midsection at Mach 0.85 and 0 deg angle of attack (AOA) for MDO wing.

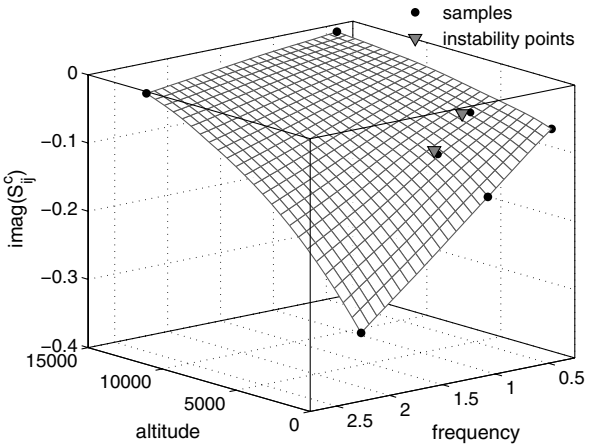

Fig. 12 Two-dimensional risk-based sampling for MDO wing configuration showing element $\mathrm{imag}(S^c_{10,1})$ of Schur interaction matrix at Mach 0.85 and 0 deg angle of attack (AOA).

altitude and frequency ranges, even though large parts of the parameter space are essentially uncovered by samples. Consequently, accurate response surfaces are not evaluated globally. There are two points to this observation. First, at high altitudes, the influence of the interaction term S^c is relatively small compared with the structural Jacobian matrix A_{ss}, as the density is relatively low. This can be observed in Figs. 8 and 12. Second, the higher frequency modes are relatively insensitive to changes in the interaction matrix elements, and the initial search space already gives a good enough approximation. Looking at the equations of the structural model and the Schur complement matrix, it is clear that the higher the normal mode frequencies, the more dominant the structural part A_{ss} on the eigenvalue problem becomes.

As for the Goland wing/store configuration, there remains a risk of missing additional (possibly more critical) instability points for the higher frequency modes. However, the cheap approximation model can be exploited to analyze the sensitivity of the eigenvalue problem with respect to the elements of the interaction matrix. Figures 13b and 13c additionally show the sensitivity of the mode tracing with respect to a 20% variation randomly distributed (in a Monte Carlo simulation) over the nonzero elements of the interaction matrix. The sensitivity is expressed as one standard deviation about the mean. In this case, the results demonstrate that the relatively large variations do not give any tendency of the six higher frequency modes to go unstable, confirming the observations in the previous paragraph, while the first and second modes give rise to some uncertainty about the onset of the instability. In addition, as the uncertainty in the aerodynamic modeling is reflected in the response surfaces, this information would allow the estimation of a necessity to use higher-fidelity (more expensive) aerodynamic modeling and, if considered to be important, the relevant locations to place the better samples.

The results of the search in three- and four-dimensional parameter spaces (related to the aerodynamic model) are shown in Fig. 14. The third dimension for the freestream Mach number covers a range between 0.7 and 0.88, while the fourth dimension for the angle of attack varies between -0.5 and $+1$ deg. Starting from the eight initial corner samples defining the three-dimensional search space, the algorithm, considering only the most critical conditions, converges rapidly and, already, the second iteration (10 samples) results in an accurate prediction, as can be seen in Fig. 14a. The problem is converged in less than seven iterations (less than 15 samples) to search the parameter space for transonic aeroelastic instabilities. It is clear that the elements of the interaction matrix are not accurately reproduced globally by the risk-based sampling. This has to be expected, considering the very low number of samples and their clustering around the first mode instability, which defines the most critical condition for this configuration to focus the search. However, locally in the region of the first mode instability, the approximation is accurate. The achieved cost reduction is

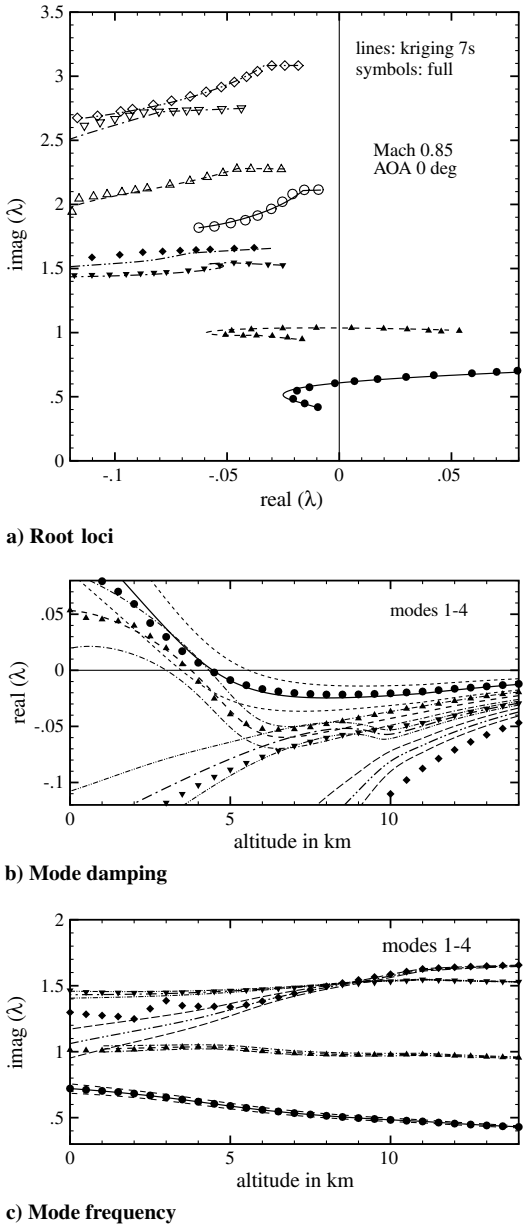

Fig. 13 Mode tracing with respect to altitude for MDO wing configuration using seven risk-based samples (7*s*) and showing sensitivity due to 20% variation in elements of interaction matrix as one standard deviation.

impressive. The 15 risk-based samples mean a cost reduction by a factor of almost 20 compared with the 256 uniformly distributed samples.

For the four-dimensional risk-based sampling, the results of which are shown in Fig. 14b, the search criterion was altered to detect all possible instability points in the specified Mach number range at a 0 deg angle of attack (following the preceding results). To be precise, rather than prescribing the lift of a trimmed condition, the angle of attack is specified. The search algorithm converges in about 14 iterations, starting from the initial 16 samples to detect the first and second mode instabilities accurately. Adding the fourth dimension to the sampling problem demonstrates an interesting point about the approach. The approximation model can be updated for changes in the system parameters by adding additional samples that account for these changes (e.g., additional samples for different angles of attack). All the previously sampled points are kept to support the prediction, as the number of samples for the approximation model grows gradually depending on the requirements. Thus, the reuse of samples is a major advantage of the kriging approach.

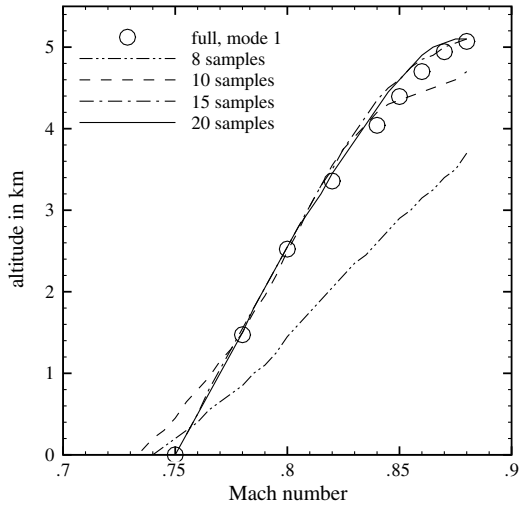

a) Three-dimensional risk-based sampling

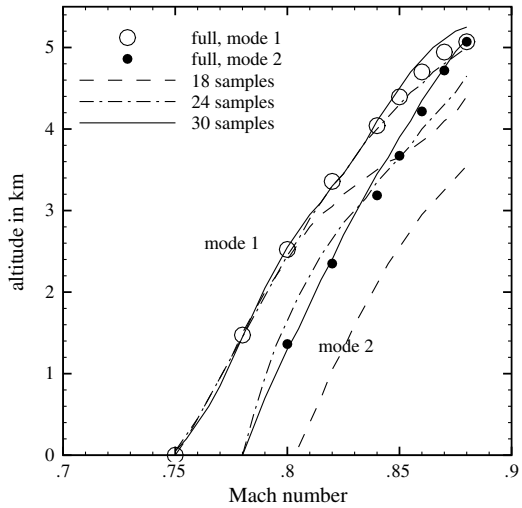

b) Four-dimensional risk-based sampling

Fig. 14 Instability boundary from three- and four-dimensional risk-based sampling for MDO wing configuration showing critical values of altitude.

V. Conclusions

The aeroelastic stability analysis based on nonlinear CFD was investigated for the linear modal structural model to describe realistic aircraft problems. Particularly, the search for aeroelastic instability over a proposed transonic flight envelope was addressed. This was demonstrated successfully by introducing searches for the approximation of the interaction matrix, modeling the influence of the aerodynamics on the modified structural eigenvalue problem solved for the stability analysis. The approximation used kriging interpolation based on exact numerical samples describing the system response. Two aircraft models were discussed, including the Goland wing and the MDO transport wing.

Using kriging interpolation based on exact numerical samples makes the approach, essentially, a model reduction technique. While the basic Schur complement eigenvalue method is faster than common time-accurate approaches, the reduced formulation proves to be computationally more efficient, despite the cost invested in the construction of the kriging model itself. The construction of the kriging model using coordinated risk-based sampling to locate new sample locations iteratively makes the approach efficient in detecting aeroelastic instability in larger parameter spaces requiring not more than the cost of several steady-state simulations (e.g., for the MDO wing undergoing static aeroelastic deformation, a transonic instability boundary in a three-dimensional search space was predicted at the cost of about 20 steady-state simulations).

Updating an approximation model with available information from flight tests must be discussed in future studies. Processed response signals provide estimates for modal frequency and damping at given parameter combinations (like freestream Mach number and altitude) within the stable flight envelope. This information could then be used, for instance, in an inverse eigenvalue problem to update the interaction matrices obtained from a high-fidelity CFD simulation. These updated matrices could provide the means to predict the instability onset beyond the flight-test limits.

Appendix

For convenience, a single scalar system response y is assumed to be a function of the m-dimensional input vector $\boldsymbol{s}$. The discussion, however, generalizes for multidimensional responses. In the current case, let y be an element S^c_{ij} of the interaction matrix and let $\boldsymbol{s}$ represent a combination of system parameters, such as frequency (i.e., imaginary part of eigenvalue) and freestream Mach number. Consider a given set of n numerical samples, $[\boldsymbol{s}_1, \ldots, \boldsymbol{s}_n]^T$, and the corresponding system response $\boldsymbol{y}_s = [y(\boldsymbol{s}_1), \ldots, y(\boldsymbol{s}_n)]^T$. The best linear unbiased predictor, referred to as the kriging predictor, minimizes the error of the interpolation [36] and is given as

$$\hat{y}(\boldsymbol{x}) = \boldsymbol{f}(\boldsymbol{x}) \cdot \boldsymbol{\beta} + \boldsymbol{r}(\boldsymbol{x}) \cdot [R^{-1}(\boldsymbol{y}_s - F\boldsymbol{\beta})] \tag{A1}$$

where the first term is the regression, while the second term adjusts the prediction based on the correlation. More important, the kriging predictor approximates the system response at an unsampled location $\boldsymbol{x}$ at the expense of only two scalar products. The gradient $\nabla\hat{y}(\boldsymbol{x})$ of the predicted response, required in solving the Schur eigenvalue problem using the Newton method, is given as

$$\nabla\hat{y}(\boldsymbol{x}) = \boldsymbol{f}_{\boldsymbol{x}}^T\boldsymbol{\beta} + \boldsymbol{r}_{\boldsymbol{x}}^T[R^{-1}(\boldsymbol{y}_s - F\boldsymbol{\beta})] \tag{A2}$$

with $\boldsymbol{f}_{\boldsymbol{x}}$ and $\boldsymbol{r}_{\boldsymbol{x}}$ expressing the analytically evaluated Jacobian matrices of the vector of basis functions $\boldsymbol{f}$ and the vector of correlations $\boldsymbol{r}$ with respect to the unsampled location $\boldsymbol{x}$.

The root-mean-squared error φ is referred to as the standard error of the kriging model and is a measure of uncertainty in the prediction. It is evaluated by

$$\varphi^2(\boldsymbol{x}) = \sigma^2[1 - \boldsymbol{r}(\boldsymbol{x}) \cdot R^{-1}\boldsymbol{r}(\boldsymbol{x}) + \boldsymbol{u} \cdot (F^TR^{-1}F)^{-1}\boldsymbol{u}] \tag{A3}$$

with the vector $\boldsymbol{u}(\boldsymbol{x}) = F^TR^{-1}\boldsymbol{r}(\boldsymbol{x}) - \boldsymbol{f}(\boldsymbol{x})$ and the process variance

$$\sigma^2 = n^{-1}(\boldsymbol{y}_s - F\boldsymbol{\beta})^TR^{-1}(\boldsymbol{y}_s - F\boldsymbol{\beta}) \tag{A4}$$

The second term in Eq. (A3) reduces the prediction error, since an unsampled location $\boldsymbol{x}$ is correlated with the known set of samples, whereas the third terms adjust for errors in estimating the regression model. More important, at a sample location, the error is zero.

The vector of regression parameters $\boldsymbol{\beta}$ is the generalized least-squares estimator of the overdetermined regression problem $\boldsymbol{y}_s \approx F\boldsymbol{\beta}$ and is given by the expression

$$\boldsymbol{\beta} = (F^TR^{-1}F)^{-1}F^TR^{-1}\boldsymbol{y}_s \tag{A5}$$

with F as regression matrix and R as the correlation matrix. The matrix $F = [\boldsymbol{f}(\boldsymbol{s}_1), \ldots, \boldsymbol{f}(\boldsymbol{s}_n)]^T$ is built from basis vectors $\boldsymbol{f}$. A constant regression gives the matrix F as a $n \times 1$ unit column vector, whereas in the linear case, the elements of the matrix are given by $\boldsymbol{f}(\boldsymbol{s}) = [1, s_1, \ldots, s_m]^T$. The matrix R of dimension $n \times n$ is built from the elements

$$R_{ij}(\boldsymbol{\theta}, \boldsymbol{p}, \boldsymbol{s}_i, \boldsymbol{s}_j) = \prod_{k=1}^{m} \mathrm{scf}(\theta_k, p_k, s_k^{(i)} - s_k^{(j)}) \tag{A6}$$

where scf is a spatial correlation function of the arguments $\boldsymbol{\theta}$, $\boldsymbol{p}$ and the distance between samples $\boldsymbol{s}_i$ and $\boldsymbol{s}_j$. Several (such as exponential and spline) correlation functions have been given in the literature, reflecting characteristics of the system output. The correlation vector

$$\boldsymbol{r}(\boldsymbol{x}) = [R_{11}(\boldsymbol{\theta}, \boldsymbol{p}, \boldsymbol{s}_1, \boldsymbol{x}), \ldots, R_{n1}(\boldsymbol{\theta}, \boldsymbol{p}, \boldsymbol{s}_n, \boldsymbol{x})]^T \tag{A7}$$

contains the correlation between the provided set of samples and an unsampled location $\boldsymbol{x}$. The parameter θ_k indicates the activity of the kth independent variable, while p_k is a measure of the smoothness in a coordinate direction. The vector of parameters $\boldsymbol{p}$ is often predefined by the chosen correlation model (such as a Gaussian-like correlation), whereas the optimal correlation coefficients $\boldsymbol{\theta}$ are given by the maximum likelihood estimate [36,41] and minimize the expression $\det(R^{1/n}\sigma^2)$. This requires the nontrivial iteration to the optimum.

Acknowledgment

This research forms part of the programme of the Marie Curie Excellence Team ECERTA, financially supported by the European Union under contract MEXT-CT-2006-042383.

References

[1] Hassig, H. J., "An Approximate True Damping Solution of the Flutter Equation by Determinant Iteration," *Journal of Aircraft*, Vol. 8, No. 11, 1971, pp. 885–889. doi:10.2514/3.44311

[2] Albano, E., and Rodden, W. P., "A Doublet-Lattice Method for Calculating Lift Distributions on Oscillating Surfaces in Subsonic Flows," *AIAA Journal*, Vol. 7, No. 2, 1969, pp. 279–285. doi:10.2514/3.5086

[3] Palacios, R., Climent, H., Karlsson, A., and Winzell, B., "Assessment of Strategies for Correcting Linear Unsteady Aerodynamics Using CFD or Experimental Results," *Progress in Computational Flow-Structure Interaction*, edited by W. Haase, V. Selmin, and B. Winzell, Springer–Verlag, New York, 2003, pp. 209–224.

[4] Yurkovich, R. N., "Status of Unsteady Aerodynamic Prediction for Flutter of High-Performance Aircraft," *Journal of Aircraft*, Vol. 40, No. 5, 2003, pp. 832–842. doi:10.2514/2.6874

[5] Ashley, H., "Role of Shocks in the "Sub-Transonic" Flutter Phenomenon," *Journal of Aircraft*, Vol. 17, No. 3, 1980, pp. 187–197. doi:10.2514/3.57891

[6] Shang, J. S., "Three Decades of Accomplishments in Computational Fluid Dynamics," *Progress in Aerospace Sciences*, Vol. 40, No. 3, 2004, pp. 173–197. doi:10.1016/j.paerosci.2004.04.001

[7] Farhat, C., Geuzaine, P., and Brown, G., "Application of a Three-Field Nonlinear Fluid-Structure Formulation to the Prediction of the Aeroelastic Parameters of an F-16 Fighter," *Computers and Fluids*, Vol. 32, No. 1, 2003, pp. 3–29. doi:10.1016/S0045-7930(01)00104-9

[8] Woodgate, M. A., Badcock, K. J., Rampurawala, A. M., and Richards, B. R., "Aeroelastic Calculations for the Hawk Aircraft Using the Euler Equations," *AIAA Journal*, Vol. 42, No. 4, 2005, pp. 1005–1012. doi:10.2514/1.5608

[9] Romanowski, M. C., "Reduced Order Unsteady Aerodynamics and Aeroelastic Models Using Karhunen–Loeve Eigenmodes," AIAA Paper 1996-3981, 1996.

[10] Hall, K. C., Thomas, J. P., and Dowell, E. H., "Proper Orthogonal Decomposition Technique for Transonic Unsteady Aerodynamic Flows," *AIAA Journal*, Vol. 38, No. 10, 2000, pp. 1853–1862. doi:10.2514/2.867

[11] Lieu, T., Farhat, C., and Lesoinne, M., "Reduced-Order Fluid/Structure Modeling of a Complete Aircraft Configuration," *Computer Methods in Applied Mechanics and Engineering*, Vol. 195, Nos. 41–43, 2006, pp. 5730–5742. doi:10.1016/j.cma.2005.08.026

[12] Lucia, D. J., Beran, P. S., and Silva, W. A., "Reduced-Order Modeling: New Approaches for Computational Physics," *Progress in Aerospace Sciences*, Vol. 40, Nos. 1–2, 2004, pp. 51–117. doi:10.1016/j.paerosci.2003.12.001

[13] Silva, W. A., and Bartels, R. E., "Development of Reduced-Order Models for Aeroelastic Analysis and Flutter Prediction Using the CFL3Dv6.0 code," *Journal of Fluids and Structures*, Vol. 19, No. 6, 2004, pp. 729–745. doi:10.1016/j.jfluidstructs.2004.03.004

[14] Hall, K. C., Thomas, J. P., and Clark, W. S., "Computation of Unsteady Nonlinear Flows in Cascades Using a Harmonic Balance Technique," *AIAA Journal*, Vol. 40, No. 5, 2002, pp. 879–886. doi:10.2514/2.1754

[15] Woodgate, M. A., and Badcock, K. J., "Implicit Harmonic Balance Solver for Transonic Flow with Forced Motions," *AIAA Journal*, Vol. 47, No. 4, 2009, pp. 893–901. doi:10.2514/1.36311

[16] Morton, S. A., and Beran, P. S., "Hopf Bifurcation Analysis Applied to Deforming Airfoils at Transonic Speeds," AIAA Paper 1997-1772, 1997.

[17] Morton, S. A., and Beran, P. S., "Hopf-Bifurcation Analysis of Airfoil Flutter at Transonic Speeds," *Journal of Aircraft*, Vol. 36, No. 2, 1999, pp. 421–429. doi:10.2514/2.2447

[18] Badcock, K. J., Woodgate, M. A., and Richards, B. E., "Hopf Bifurcation Calculations for a Symmetric Airfoil in Transonic Flow," *AIAA Journal*, Vol. 42, No. 5, 2004, pp. 883–892. doi:10.2514/1.9584

[19] Badcock, K. J., Woodgate, M. A., and Richards, B. E., "Direct Aeroelastic Bifurcation Analysis of a Symmetric Wing Based on Euler Equations," *Journal of Aircraft*, Vol. 42, No. 3, 2005, pp. 731–737. doi:10.2514/1.5323

[20] Woodgate, M. A., and Badcock, K. J., "Fast Prediction of Transonic Aeroelastic Stability and Limit Cycles," *AIAA Journal*, Vol. 45, No. 6, 2007, pp. 1370–1381. doi:10.2514/1.25604

[21] Badcock, K. J., and Woodgate, M. A., "Bifurcation Prediction of Large-Order Aeroelastic Models," *AIAA Journal*, Vol. 48, No. 6, 2010, pp. 1037–1046. doi:10.2514/1.40961

[22] Marques, S., Badcock, K. J., Khodaparast, H. H., and Mottershead, J. E., "On how Structural Model Variability Influences Transonic Aeroelastic Stability," AIAA Paper 2010-3047, 2010.

[23] Marques, S., Badcock, K. J., Khodaparast, H. H., and Mottershead, J. E., "Transonic Aeroelastic Stability Predictions Under the Influence Of Structural Variability," *Journal of Aircraft*, Vol. 47, No. 4, 2010, pp. 1229–1239. doi:10.2514/1.46971

[24] Timme, S., and Badcock, K. J., "Searching for Transonic Aeroelastic Instability Using an Aerodynamic Model Hierarchy," AIAA Paper 2010-3048, 2010.

[25] Badcock, K. J., Richards, B. E., and Woodgate, M. A., "Elements of Computational Fluid Dynamics on Block Structured Grids Using Implicit Solvers," *Progress in Aerospace Sciences*, Vol. 36, Nos. 5–6, 2000, pp. 351–392. doi:10.1016/S0376-0421(00)00005-1

[26] Osher, S., and Chakravarthy, S. R., "Upwind Schemes and Boundary Conditions with Applications to Euler Equations in General Geometries," *Journal of Computational Physics*, Vol. 50, No. 3, 1983, pp. 447–481. doi:10.1016/0021-9991(83)90106-7

[27] van Leer, B., "Towards the Ultimative Conservative Difference Scheme, V: A Second-Order Sequel to Godunov's Method," *Journal of Computational Physics*, Vol. 32, No. 1, 1979, pp. 101–136. doi:10.1016/0021-9991(79)90145-1

[28] Jameson, A., "Time Dependent Calculations Using Multigrid with Applications to Unsteady Flows Past Airfoils and Wings," AIAA Paper 1991-1596, 1991.

[29] Goura, G. S. L., "Time Marching Analysis of Flutter Using Computational Fluid Dynamics," Ph.D. Thesis, Department of Aerospace Engineering, Univ. of Glasgow, Glasgow, Scotland, U.K., 2001.

[30] Wright, J. R., and Cooper, J. E., *Introduction to Aircraft Aeroelasticity and Loads*, Wiley, Chichester, England, U.K., 2007, pp. 171–172.

[31] Eisenstat, S. C., Elman, H. C., and Schultz, M., "Variational Iterative Methods for Nonsymmetric Systems of Linear Equations," *SIAM Journal on Numerical Analysis*, Vol. 20, No. 2, 1983, pp. 345–357. doi:10.1137/0720023

[32] Bekas, C., and Saad, Y., "Computation of Smallest Eigenvalues Using Spectral Schur Complements," *SIAM Journal on Scientific Computing*, Vol. 27, No. 2, 2005, pp. 458–481. doi:10.1137/040603528

[33] Bakhle, M. A., Mahajan, A. J., Keith, T. G., Jr., and Stefko, G. L., "Cascade Flutter Analysis with Transient Response Aerodynamics," *Computers and Structures*, Vol. 41, No. 5, 1991, pp. 1073–1085. doi:10.1016/0045-7949(91)90302-3

[34] Silva, W. A., "Simultaneous Excitation of Multiple-Input/Multiple-Output CFD-Based Unsteady Aerodynamic Systems," *Journal of Aircraft*, Vol. 45, No. 4, 2008, pp. 1267–1274. doi:10.2514/1.34328

[35] Jones, D. R., Schonlau, M., and Welch, W. J., "Efficient Global Optimization of Expensive Black-Box Functions," *Journal of Global Optimization*, Vol. 13, No. 4, 1998, pp. 455–492.

doi:10.1023/A:1008306431147
[36] Sacks, J., Welch, W. J., Mitchell, T. J., and Wynn, H. P., "Design and Analysis of Computer Experiments," *Statistical Science*, Vol. 4, No. 4, 1989, pp. 409–435.
doi:10.1214/ss/1177012413
[37] Lophaven, S. N., Nielsen, H. B., and Soendergaard, J., "DACE: A Matlab Kriging Toolbox," Technical Univ. of Denmark, TR IMM-TR-2002-12, Kongens Lyngby, Denmark, 2002.
[38] Rodden, W. P., and Johnson, E. H., "MSC.Nastran Aeroelastic Analysis User's Guide," MSC.Software Corp., Santa Ana, CA, 2004.
[39] Beran, P. S., Khot, N. S., Eastep, F. E., Snyder, R. D., and Zweber, J. V., "Numerical Analysis of Store-Induced Limit-Cycle Oscillation," *Journal of Aircraft*, Vol. 41, No. 6, 2004, pp. 1315–1326.
doi:10.2514/1.404
[40] Bendiksen, O. O., "Transonic Limit Cycle Flutter of High-Aspect-Ratio Swept Wings," *Journal of Aircraft*, Vol. 45, No. 5, 2008, pp. 1522–1533.
doi:10.2514/1.29547
[41] Welch, W. J., Buck, R. J., Sacks, J., Wynn, H. P., Mitchell, T. J., and Morris, M. D., "Screening, predicting, and computer experiments," *Technometrics*, Vol. 34, No. 1, 1992, pp. 15–25.
doi:10.2307/1269548

L. Tichy
Associate Editor